Synthesis, Structures, and Kinetics and Mechanism of Decomposition of Terminal Metal Azide Complexes: Isolated Intermediates in the Formation of Imidometal Complexes from Organic Azides

Grant Proulx and Robert G. Bergman*

Department of Chemistry, University of California, Berkeley, California 94720

Received October 10, 1995[⊗]

Treatment of $Cp_2Ta(CH_3)(PMe_3)$ ($Cp = \eta^5$-C_5H_5) with aryl azides ArN_3 ($Ar = C_6H_5$, p-$CF_3C_6H_4$, p-$NMe_2C_6H_4$) affords rare examples of terminal phenylazido complexes $Cp_2Ta(CH_3)(N_3Ar)$ and free phosphine in >85% yield. $Cp_2Ta(CH_3)(N_3C_6H_5)$ (**1a**) crystallizes in the space group $P2_1$ with the following parameters: $a = 6.6838(13)$ Å, $b = 13.4491(17)$ Å, $c = 20.082(3)$ Å, $\beta = 98.714(14)°$, $V = 1784.4(9)$ Å^3, $Z = 4$, $R = 2.36\%$, and $R_w = 2.82\%$. $Cp_2Ta(CH_3)(N_3$-p-NMe_2-$C_6H_4)$ (**1b**) crystallizes in the space group $Pna2_1$ with the following parameters: $a = 23.275(5)$ Å, $b = 6.497(2)$ Å, $c = 11.621(2)$ Å, orthorhombic, $V = 1757.3(12)$ Å^3, $Z = 4$, $R = 1.53\%$, and $R_w = 1.70\%$. Heating the terminal azide complexes to 70 °C for several hours or subjecting them to UV irradiation for minutes affords dinitrogen and the previously characterized imido species $Cp_2Ta(CH_3)(=NAr)$ in quantitative yield. Treatment of the α-^{15}N-labeled azide Ph-^{15}N=N=N with $Cp_2Ta(PMe_3)(CH_3)$ gives $Cp_2Ta(NN^{15}NPh)(CH_3)$, and thermolysis of this material leads to $Cp_2Ta(CH_3)(^{15}NPh)$. This shows conclusively that the nitrogen atom that is originally bound to the Ta center is incorporated into the free N_2 product. A double-labeling experiment was also undertaken in which equimolar amounts of $Cp_2Ta(^{13}CH_3)(NNNPh)$ and $Cp_2Ta(CH_3)(NN^{15}NPh)$ were shown to give only the singly labeled imido species $Cp_2Ta(CH_3)(^{15}NPh)$ and $Cp_2Ta(^{13}CH_3)(NPh)$. The rate of decomposition of the azide complexes was strongly affected by traces of air. However, in the presence of the powerful O_2 and H_2O scavenger $Cp_2Zr(CH_3)_2$, the conversion of $Cp_2Ta(CH_3)(N_3C_6H_5)$ to $Cp_2Ta(CH_3)(=NC_6H_5)$ was found to be first order in $[Cp_2Ta(CH_3)(N_3C_6H_5)]$ at all concentrations and temperatures examined. Rates measured over a 40 °C temperature range gave Eyring parameters $\Delta H^{\ddagger} = 25.4$ kcal/mol and $\Delta S^{\ddagger} = -0.7$ eu. A Hammett σ/ρ investigation using para-substituted phenylazido complexes demonstrated that the rate of dinitrogen loss is accelerated by the presence of electron-withdrawing groups on the azide nitrogen. The mechanistic implications of these results are discussed.

In recent years chemists have become increasingly interested in transition metal imido species because of the wide range of reactions these systems have been observed to undergo.[1] A number of complexes containing the M=NR fragment are so reactive that in some cases they will even activate C−H bonds.[2−4] One of the most commonly used methods for generating imido species involves treatment of metal complexes with organic azides (RN_3), nitrogen-containing compounds that have been used by organic chemists for years as convenient sources of "RN:" or nitrene fragments.[5] In the synthesis of imidometal species, organoazidometal complexes were proposed as intermediates formed in the initial interaction of a coordinately unsaturated metal complex with RN_3.[6−10] There are some examples of RN_3X complexes that are stabilized by insertion of the RN_3 group into a M−X bond (to obtain complexes like cyclic $L_nM(\eta^2$-$N(=PR_3)N=NR')$)[9,11] and other examples of structurally characterized RN_3 complexes bridging two metal centers,[12] but at the start of this work there did not appear to be any monometallic MN_3R complexes whose structures had been established by X-ray diffraction. In a few reported instances when transition metal alkyls were allowed to react with aryl azides, 1,3-disubstituted triazenido complexes ($L_nMNRN=NR$) result,[11] or in a case where N_2 is lost, nitrene fragment insertion into the M−C bond to form the corresponding amido−metal complex is observed.[13] However, there are few examples of reactions that yield simple intact (organoazido)metal complexes, presumably due to their rapid loss of N_2.[7,8]

[⊗] Abstract published in *Advance ACS Abstracts,* December 15, 1995.

(1) (a) Nugent, W. A.; Mayer, J. M. *Metal-Ligand Multiple Bonds*; John Wiley and Sons: New York, 1988. (b) Wigley, D. E. *Prog. Inorg. Chem.* **1994**, *42*, 239.
(2) Cummins, C. C.; Baxter, S. M.; Wolczanski, P. T. *J. Am. Chem. Soc.* **1988**, *110*, 8731.
(3) Walsh, P. J.; Hollander, F. J.; Bergman, R. G. *J. Am. Chem. Soc.* **1988**, *110*, 8731.
(4) Cummins, C. C.; Schaller, C. P.; VanDuyne, G. D.; Wolcazanski, P. T.; Chan, A. W. E.; Hoffman, R. *J. Am. Chem. Soc.* **1991**, *113*, 2985.
(5) Lwowski, W. *Nitrenes*; Interscience Publishers: New York, 1970.
(6) Hillhouse, G. L.; Haymore, B. L. *J. Am. Chem. Soc.* **1982**, *104*, 1537.
(7) Antonelli, D. M.; Schaefer, W. P.; Parkin, G.; Bercaw, J. E. *J. Organomet. Chem.* **1993**, *462*, 213.
(8) Gambarotta, S.; Chiesi-Villa, A.; Guastini, C. *J. Organomet. Chem.* **1984**, *270*, C49.
(9) Hillhouse, G. L.; Goeden, G. V.; Haymore, B. L. *Inorg. Chem.* **1982**, *21*, 2064.
(10) Rosen, R. K. Ph.D. Thesis, U.C. Berkeley, Berkeley, CA, 1989.
(11) Chiu, K. W.; Wilkinson, G.; Thornton-Pett, M.; Hursthouse, M. *Polyhedron* **1984**, *3*, 79.
(12) Hanna, T. A.; Bergman, R. G. *Angew. Chem.*, submitted for publication.
(13) Matsunaga, P. T.; Hess, C. R.; Hillhouse, G. L. *J. Am. Chem. Soc.* **1994**, *116*, 3665.

0276-7333/96/2315-0684$12.00/0

We previously reported the isolation and full characterization of a terminal (organoazido)metal complex, $Cp_2Ta(N_3Ph)(CH_3)$ (**1**).[14,15] This report extends our work to encompass several other (arylazido)tantalum complexes and describes the full experimental details of the synthesis, isolation, and structural characterization of these $Cp_2Ta(N_3Ar)(CH_3)$ species. We also report mechanistic experiments that shed light on the pathway for conversion of these complexes to the corresponding terminal imidometal species, $Cp_2Ta(NAr)(CH_3)$, along with kinetics of N_2 loss and isotopic and group-substitution labeling studies that bear on the transition state of decomposition of the arylazidotantalum complexes.

Results

Treatment of a toluene solution of the known red Ta(III) species $Cp_2Ta(PMe_3)(CH_3)$[16] ($Cp = \eta^5$-C_5H_5) with PhN_3 at room temperature causes a rapid color change to deep orange. Monitoring this reaction by ^1H and ^{31}P NMR spectroscopy shows the formation of free PMe_3 and a new species in essentially quantitative yield with the formula $Cp_2Ta(N_3Ph)(CH_3)$ (**1a**) (eq 1). The ^1H NMR

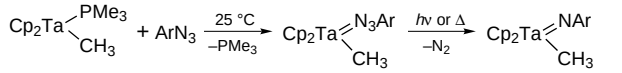

1 **2**

a, Ar = C_6H_5
b, Ar = *p*-$NMe_2C_6H_4$
c, Ar = *p*-$CF_3C_6H_4$ (1)

spectrum of **1a** shows a single resonance at δ 5.21, indicating equivalent cyclopentadienyl rings along with a CH_3 group at δ 0.54. On the basis of its chemical shift at δ 0.54, it is clear that the Me group has not migrated to a nitrogen atom. Three aromatic proton resonances are observed as well. Orange needlelike crystals of **1a** were obtained by benzene/pentane vapor diffusion to give pure $Cp_2Ta(N_3Ph)(CH_3)$ in 88% yield. The IR spectrum of these crystals shows a strong absorbance for a N═N double bond at 1730 cm^{-1}.

1a is stable at room temperature in solution and in the solid state in the dark for weeks in the absence of air or water. When this compound is subjected to high vacuum for several hours, no change in the spectroscopic properties of **1a** is observed nor is there any observation of free azide or dinitrogen effervescence. In the solid state, **1a** decomposes with apparent dinitrogen extrusion at 105° C. In C_6D_6 solution, however, **1a** loses N_2 over the course of several hours at 70 °C to give the previously characterized imido complex, $Cp_2Ta(═NPh)(CH_3)$ (**2a**),[17] in quantitative isolated yield (>95% ^1H NMR vs Cp_2Fe internal standard). Upon photolysis of complex **1a** in solution in a quartz vessel or in the solid state, dinitrogen effervescence is observeed and **2a** is also rapidly formed quantitatively over the course of minutes.

Despite the spectroscopic evidence for an organoazide complex, it was still ambiguous whether the azide ligand was bound in an η^2−olefinic mode (A, Figure 1), an η^2-triazametallacyclobutene mode (B), an η^1-terminal mode (C), or an η^1-diazoamide mode (D). In order to resolve this ambiguity, a single-crystal X-ray diffraction study of **1a** was undertaken. The structure was solved by Patterson methods in space group $P2_1$ and refined via standard least-squares and Fourier techniques. The bonding and molecular geometry of **1a** are shown in an ORTEP diagram in Figure 2, and the crystallographic data and parameters for **1a** are given in Table 1 with positional parameters in Table 2 and selected bond distances and angles in Table 3. As the structure shows, the azide ligand adopts an η^1-terminal configuration (C, Figure 1) in the solid state. It does not prefer a cyclic configuration, which would allow the metal to interact with two nitrogens of the ligand, nor does the molecule opt for an olefinic type bonding mode analogous to the previously characterized η^2-S_2 and η^2-C_2H_4 complexes in this species.[16,17]

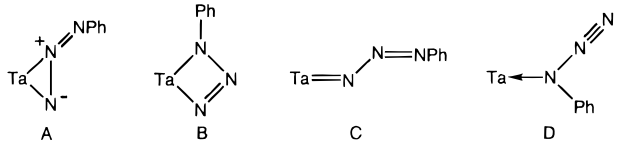

Figure 1. Possible binding modes for a tantalum azide complex: (A) η^2-olefinic mode; (B) η^2-triazametallacyclobutene mode; (C) η^1-terminal mode; (D) η^1-diazophenylamino mode.

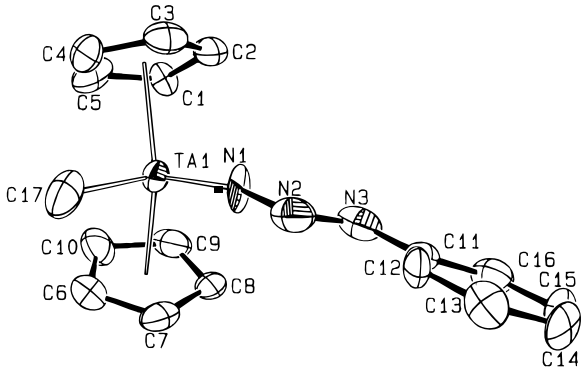

Figure 2. ORTEP diagram of one of the two crystallographically independent molecules of $Cp_2Ta(CH_3)(N_3C_6H_5)$ (**1a**).

In the crystal structure, there are a total of four molecules of the compound and two molecules of benzene in the unit cell, and there are no abnormally short intermolecular contacts between the molecules. The bonding of the methyl and the Cp ligands to the tantalum appears to be normal, but the formal bonding arrangement of the N_3 ligand is a little less obvious.[18,19] The Ta−N−N angle in **1a** (166.0(10)°) is bent more strongly than in the tantalum phenylimido species, $Cp^*_2Ta(═NPh)(H)$, where ∠Ta−N−C is 177.8(9)°.[18] The Ta═N bonding distance (the two independent molecules in the unit cell are similar at 1.830(11) and 1.845(10) Å) is also significantly shorter than in those compounds viewed as having "true" Ta═N double bonds (estimated by Bercaw and co-workers as ca. 1.89 Å) and significantly longer than for those having "true" Ta≡N triple bonds (1.75 Å).[18,20] It therefore appears that the most

(14) Proulx, G.; Bergman, R. G. *J. Am. Chem. Soc.* **1995**, *117*, 6382.
(15) In a related vanadium organoazide complex discovered simultaneously and independently by Cummins and co-workers, different behavior was observed regarding the azide ligand. In Cummins' system, rapid scrambling of free azide into the bound azide position was found, and second-order kinetics were also observed. Our system does not seem to display either of these characteristics. See: Cummins, C. C.; Fickes, M. J.; Davis, W. M. *J. Am. Chem. Soc.* **1995**, *117*, 6384.
(16) Schrock, R. R.; Sharp, P. R. *J. Am. Chem. Soc.* **1978**, *100*, 2389.
(17) Proulx, G.; Bergman, R. G. *J. Am. Chem. Soc.* **1994**, *116*, 7953.
(18) Parkin, G.; van Asselt, A.; Leahy, D. J.; Whinnery, L.; Hua, N. G.; Quan, R. W.; Henling, L. M.; Schaefer, W. P.; Santarsiero, B. D.; Bercaw, J. E. *Inorg. Chem.* **1992**, *31*, 82.
(19) Jørgensen, K. A. *Inorg. Chem.* **1993**, *32*, 1521.

Table 1. Crystallographic Data Collection and Crystal Parameters for $Cp_2(CH_3)Ta(N_3(C_6H_5))\cdot 0.5(C_6H_6)$ (1a) and $Cp_2(CH_3)Ta(N_3(C_6H_4NMe_2)$ (1b)

	1a	1b
Crystal Parameters[a,b]		
formula	$TaN_3C_{20}H_{21}$	$TaN_4C_{19}H_{23}$
formula weight	484.4	488.4
crystal syst	monoclinic	orthorhombic
space group	$P2_1$	$Pna2_1$
Z	4	4
a, Å	6.6838(13)	23.275(5)
b, Å	13.4491(17)	6.497(2)
c, Å	20.082(3)	11.621(2)
β°	98.714(14)	90.0
V, Å^3	1784.4(9)	1757.3(12)
d_{calc}, g cm^{-3}	1.80	1.85
cryst dimens, mm	0.07 × 0.20 × 0.34	0.10 × 0.30 × 0.40
T, °C	−115	−111
Measurement of Intensity Data		
radiation (monochrome)	Mo Kα (λ = 0.710 73 Å) graphite	Mo Kα (λ = 0.710 73 Å) graphite
scan type	$\theta-2\theta$	ω
scan rate, deg/min	5.49	8.24
2θ range, deg	3−45	3−48
data collected	$+h,+k,\pm l$	$\pm h,+k,+l$
no. of data collected	2469	2996
no. of unique data ($F^2 > 3\sigma(F^2)$)	2443	1456
no. of variables	427	216
μ_{calc}, cm^{-1}	60.9	61.9
R	0.0236	1.53
R_w	0.0282	1.70
GOF	1.297	0.69

[a] Unit cell parameters and their esd's were derived by a least-squares fit to the setting angles of the unresolved Mo Kα components of 24 reflections with 2θ between 28° and 32°. [b] In this table the esd's of all parameters are given in parentheses, right-justified to the least significant digit(s) of the reported value.

reasonable picture of the bonding situation at the metal center postulates a situation intermediate between double and triple bonding. The PhN═N bond length of 1.267(15) Å is slightly longer than typical N═N double bonds, such as that in *trans*-azobenzene (1.247(2) Å).[21] As a note of caution with respect to these numbers, however, upon inspection of the thermal parameters for the N_3 ligand it appeared there was some peculiar "thermal motion" which was observed with respect to the organoazide ligand on one of the two crystallographically independent molecules in the structure. This may represent the effect of the interaction of the molecule with the X-rays passing through the structure (possibly extruding N_2 at −115 °C but not allowing the molecule to escape from the lattice) plus damage to the crystal which occurred during its brief exposure to the warm Paratone N while attempting to mount it. For this reason, we recommend that the distances and angles in the region of the molecule with respect to N5 and N6 be interpreted with some care. The final residuals, however, were quite good for 427 variables refined against the 2277 accepted data for which $F^2 > 3\sigma(F^2)$ at R = 2.36% and wR = 2.82% with a GOF of 1.297.

Because of the peculiar "thermal motion" observed in **1a** and because of the novelty of the terminal azide ligand, we wanted more precise information about the bond lengths in the tantalum azide ligand. For this reason, we synthesized other substituted tantalum azides including $Cp_2Ta(CH_3)(N_3(p\text{-}NMe_2\text{-}C_6H_4))$ (**1b**) and $Cp_2Ta(CH_3)(N_3(p\text{-}CF_3\text{-}C_6H_4))$ (**1c**). Both of these compounds were synthesized in a fashion similar to that

Table 2. Positional Parameters and Their Estimated Standard Deviations for $Cp_2Ta(CH_3)(N_3C_6H_5)$ (1a)[a]

atom	x	y	z	B (Å^2)
Ta1	0.34506(6)	0.00	0.48795(1)	2.231(8)
Ta2	−0.15740(6)	−0.28093(1)	0.00386(1)	2.280(8)
N1	0.549(1)	−0.0817(7)	0.5291(5)	3.6(2)
N2	0.706(2)	−0.1196(8)	0.5647(5)	4.3(2)
N3	0.669(2)	−0.1782(7)	0.6108(5)	3.6(2)
N4	0.006(1)	−0.3660(7)	−0.0343(4)	3.2(2)*
N5	0.158(2)	−0.413(1)	−0.0728(6)	8.4(4)
N6	0.057(2)	−0.4614(9)	−0.1107(6)	5.5(3)
C1	0.037(2)	−0.0758(8)	0.4396(5)	2.2(2)
C2	0.192(2)	−0.1515(9)	0.4387(6)	4.1(3)
C3	0.323(2)	−0.119(1)	0.3976(6)	3.4(3)
C4	0.239(2)	−0.0245(9)	0.3680(5)	3.3(3)
C5	0.063(2)	−0.005(1)	0.3937(5)	3.7(3)
C6	0.340(2)	0.1654(9)	0.5344(6)	3.6(3)
C7	0.442(2)	0.106(1)	0.5848(6)	3.9(3)
C8	0.302(2)	0.0370(9)	0.6039(5)	4.1(3)
C9	0.114(2)	0.0524(9)	0.5635(6)	3.8(3)
C10	0.135(2)	0.1327(9)	0.5199(6)	3.8(3)
C11	0.861(2)	−0.2173(8)	0.6492(5)	2.8(2)
C12	1.050(2)	−0.2056(9)	0.6333(5)	3.4(3)
C13	1.216(2)	−0.2443(9)	0.6753(6)	3.7(3)
C14	1.189(2)	−0.2985(9)	0.7318(6)	3.5(3)
C15	0.994(2)	−0.3094(9)	0.7453(6)	3.5(3)
C16	0.832(2)	−0.270(1)	0.7053(5)	3.5(3)
C17	0.568(2)	0.091(1)	0.4369(6)	4.4(3)
C21	−0.149(2)	−0.1791(9)	−0.0972(6)	4.3(3)
C22	−0.200(2)	−0.1148(9)	−0.0437(6)	3.6(3)
C23	−0.388(2)	−0.1459(8)	−0.0311(5)	2.6(2)
C24	−0.453(2)	−0.230(1)	−0.0718(6)	4.3(3)
C25	−0.302(2)	−0.2469(9)	−0.1122(6)	3.5(3)
C26	−0.417(2)	−0.3606(9)	0.0503(5)	3.4(3)
C27	−0.364(2)	−0.283(1)	−0.0946(5)	3.2(2)
C28	−0.163(2)	−0.2976(9)	0.1240(5)	3.3(3)
C29	−0.099(2)	−0.391(1)	0.1013(6)	3.3(3)
C30	−0.266(2)	−0.4312(9)	0.0558(6)	3.8(3)
C31	0.231(2)	−0.5032(9)	−0.1487(5)	3.3(2)
C32	0.432(2)	−0.497(1)	−0.1344(5)	4.5(3)
C33	0.554(2)	−0.537(1)	−0.1747(7)	5.0(3)
C34	0.469(2)	−0.590(1)	−0.2324(6)	5.7(3)
C35	0.264(2)	−0.597(1)	−0.2461(6)	5.0(4)
C36	0.144(2)	−0.556(1)	−0.2048(6)	4.1(3)
C37	0.101(2)	−0.190(1)	0.0545(6)	4.2(3)
C41	0.218(2)	−0.318(1)	0.2622(6)	4.5(3)
C42	0.380(2)	−0.348(1)	0.2340(6)	4.2(3)
C43	0.419(2)	−0.445(1)	0.2230(7)	4.5(3)
C44	0.281(3)	−0.515(1)	0.2410(7)	6.6(4)
C45	0.117(2)	−0.483(1)	0.2711(7)	5.9(4)
C46	0.087(2)	−0.385(1)	0.2821(7)	4.8(3)

[a] Starred atom was included with isotropic thermal parameters. The thermal parameter given for anisotropically refined atoms is the isotropic equivalent thermal parameter defined as $(4/3)[a^2\beta(1,1) + b^2\beta(2,2) + c^2\beta(3,3) + ab(\cos\gamma)\beta(1,2) + ac(\cos\beta)\beta(1,3) + bc(\cos\alpha)\beta(2,3)]$, where a, b, c are real cell parameters and $\beta(i,j)$ are anisotropic betas.

Table 3. Selected Intramolecular Distances and Angles for for $Cp_2Ta(CH_3)(N_3C_6H_5)$ (1a)

Distance (Å)			
Ta1−N1	1.845(10)	Ta2−N4	1.830(11)
Ta1−C17	2.286(18)	Ta2−C37	2.232(15)
N1−N2	1.282(16)	N4−N5	1.501(23)
N2−N3	1.267(15)	N5−N6	1.143(17)
N3−C11	1.489(15)	N6−C31	1.587(19)
Angle (deg)			
N1−Ta1−C17	91.8(6)	N4−Ta2−C37	93.5(5)
Ta1−N1−N2	166.5(11)	Ta2−N4−N5	166.0(10)
N1−N2−N3	115.0(12)	N4−N5−N6	102.0(18)
N2−N3−C11	110.7(12)	N5−N6−C31	97.0(15)

(20) Nugent, W. A.; Harlow, R. L. *J. Chem. Soc., Chem. Commun.* **1978**, 579.
(21) Bouwstra, J. A.; Schouten, A.; Kroon, J. *Acta Crystallogr., C* **1983**, *39*, 1121.

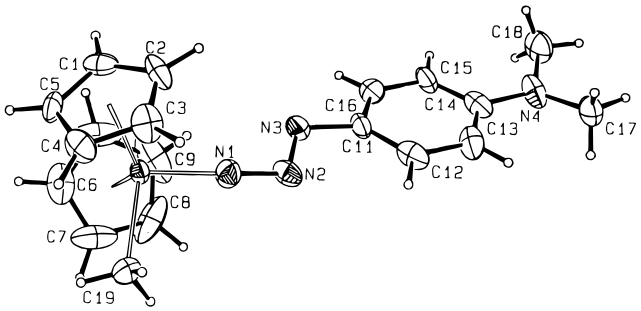

Figure 3. ORTEP diagram of $Cp_2Ta(CH_3)(N_3C_6H_4$-*p*-$NMe_2)$ (**1b**).

Table 4. Positional Parameters and Their Estimated Standard Deviations for $Cp_2Ta(CH_3)(N_3C_6H_4NMe_2)$ (1b)[a]

atom	*x*	*y*	*z*	*B* (Å^2)
Ta	0.06661(1)	0.17611(1)	0.250	1.789(4)
N1	0.0986(3)	0.380(1)	0.3414(5)	2.7(1)
N2	0.1113(2)	0.499(1)	0.4290(5)	2.6(1)
N3	0.1242(3)	0.400(1)	0.5202(b)	2.6(1)
N4	0.2147(3)	0.852(1)	0.8896(6)	3.7(2)
C1	0.1335(3)	−0.101(1)	0.2239(6)	2.8(2)
C2	0.1667(3)	0.076(1)	0.2306(6)	3.2(2)
C3	0.1537(3)	0.193(1)	0.1348(7)	3.4(2)
C4	0.1137(3)	0.088(1)	0.0695(6)	3.0(2)
C5	0.1018(3)	−0.097(1)	0.1225(7)	2.5(2)
C6	−0.0148(3)	−0.056(1)	0.266(1)	3.9(2)
C7	−0.0368(3)	0.139(1)	0.275(1)	4.6(2)
C8	−0.0146(4)	0.220(1)	0.3744(9)	5.5(2)
C9	0.0211(4)	0.082(2)	0.4252(7)	5.8(3)
C10	0.0217(3)	−0.091(1)	0.3565(9)	5.0(2)
C11	0.1427(3)	0.532(1)	0.6105(6)	2.3(2)
C12	0.1609(3)	0.738(1)	0.5875(7)	3.1(2)
C13	0.1839(3)	0.842(1)	0.6914(7)	3.3(2)
C14	0.1885(3)	0.751(1)	0.8008(7)	3.1(2)
C15	0.1696(3)	0.550(1)	0.8098(7)	3.1(2)
C16	0.1465(3)	0.450(1)	0.7184(5)	2.6(2)
C17	0.2424(4)	1.048(1)	0.8705(8)	4.1(2)
C18	0.2289(4)	0.741(1)	0.9929(8)	4.0(2)
C19	0.0271(4)	0.389(1)	0.1226(8)	3.6(2)

[a] The thermal parameter given for anisotropically refined atoms is the isotopic equivalent thermal parameter defined as $(4/3)[a^2\beta(1,1) + b^2\beta(2,2) + c^2\beta(3,3) + ab(\cos\gamma)\beta(1,2) + ac(\cos\beta)\beta(1,3) + bc(\cos\alpha)\beta(2,3)]$, where *a*, *b*, and *c* are real cell parameters and $\beta(i,j)$ are anisotropic betas.

used for the parent species **1a**. Each compound exhibited thermal stability at room temperature similar to **1a**, and they had spectral characteristics analogous to the parent species as well.

A single-crystal X-ray diffraction study of **1b** was performed. The structure was solved in space group $Pna2_1$, and the bonding and molecular geometry of **1b** are shown in an ORTEP diagram in Figure 3. The crystallographic data and parameters for **1b** are given in Table 1 with positional parameters in Table 4 and selected bond distances and angles in Table 5. As in **1a**, the azide ligand prefers an end-on position when bound to the tantalum.

In the solid state, there are a total of four molecules of the compound in the unit cell with no evidence for π-stacking interactions or abnormally short intermolecular distances. The $Ta-N_1-N_2$ bonding angle in **1b** (162.8(6)°) is slightly more bent than that in **1a**. The rest of the N_3 moiety is planar and bent slightly away from the coordination plane of the tantalum. The N_1-N_2 (1.310(9) Å) and N_2-N_3 (1.276(9) Å) distances are quite similar, suggesting significant delocalization of the bonding. The bonding around N_4 is also clearly delocalized. The structures of **1a** and **1b** are similar (within

Table 5. Selected Intramolecular Distances and Angles for $Cp_2Ta(CH_3)(N_3C_6H_4NMe_2)$ (1b)

	Distance (Å)		
Ta−N1	1.856(7)	C12−C13	1.391(21)
Ta−C19	2.224(10)	C13−C14	1.407(14)
N1−N2	1.310(9)	C14−C15	1.381(19)
N2−N3	1.276(9)	C15−C16	1.356(10)
N3−C11	1.424(10)	N4−C14	1.368(18)
C11−C12	1.410(14)	N4−C17	1.440(12)
C11−C16	1.366(12)	N4−C18	1.439(12)
	Angle (deg)		
N1−Ta−C19	95.9(3)	C12−C11−C16	116.7(8)
N1−Ta−CP1	108.3	C11−C12−C13	119.5(10)
N1−Ta−CP2	107.0	C12−C13−C14	122.2(14)
C19−Ta−CP1	103.7	N4−C14−C13	120.8(17)
C19−Ta−CP2	103.2	N4−C14−C15	122.7(16)
CP1−Ta−CP2	132.5	C13−C14−C15	116.3(13)
Ta−N1−N2	162.8(6)	C14−C15−C16	121.2(12)
N1−N2−N3	113.7(8)	C15−C16−C11	124.0(9)
N2−N3−C11	112.2(7)	C14−N4−C17	120.6(12)
N3−C11−C12	125.8(8)	C14−N4−C18	119.3(11)
N3−C11−C16	117.4(9)	C17−N4−C18	117.9(8)

experimental error) in all other respects with regards to the TaN_3 fragment. The structure of **1b** does not show the peculiar thermal motion of the azide ligand that **1a** showed and thus provides more assurance that the conclusions drawn from the bond distances and angles of the TaN_3 moiety are correct.

Monitoring a solution of **1a** by variable-temperature ^{1}H NMR spectrometry revealed no significant changes in the spectrum (THF-d_8), and all resonances remained sharp from room temperature to −50 °C. Also, addition of excess PhN_3 to a solution of $Cp_2Ta(PMe_3)(CH_3)$ at ambient temperatures leads to **1a** and to the extrusion of N_2 (evident by effervescence during addition) and the formation of $PhN{=}PMe_3$. Although we have not attempted kinetic studies, the fact that $PhN{=}PMe_3$ is not formed in the 1:1 reaction of **1a** with PhN_3 suggests strongly that it is an associative process.

We further tested the stability of the azide complex by addition of labeled azide to a solution of **1a**. Addition of excess N_3-*p*-$NMe_2C_6H_4$, N_3-*p*-$CF_3C_6H_4$, or $NN^{15}NC_6H_5$ to **1a** in C_6D_6 (eq 2) led to no incorporation (<5% by ^{1}H

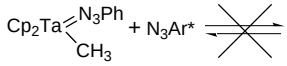

(2)

NMR) of the labeled azides into the tantalum-bound azide position over a period of 1 day at room temperature.

Isotopic labeling and kinetic studies were employed to shed light on the decomposition path of the tantalum azide. On treatment of the (>98%) α-^{15}N-labeled azide $Ph^{15}N{=}N{=}N$ with $Cp_2Ta(PMe_3)(CH_3)$, we were able to isolate the ^{15}N-labeled $Cp_2Ta(NN^{15}NPh)(CH_3)$ (**1a**-^{15}N) product and watch the further decomposition of this complex to the labeled imido species **2a**-^{15}N (>98% by FAB MS). This showed conclusively that the nitrogen atom that is originally bound to the Ta center is incorporated into free N_2. Also, a double-labeling experiment was undertaken in which we labeled both the tantalum fragment and the azide fragment. We synthesized and isolated both ^{13}C-labeled **1a**, $Cp_2Ta(^{13}CH_3)(NNNPh)$ (99% ^{13}C) (**1a**-^{13}C), and ^{15}N-labeled **1a**, $Cp_2Ta(CH_3)(NN^{15}NPh)$ (**1a**-^{15}N) (>98% ^{15}N). We then heated a C_6D_6 solution containing a 1:1 mixture of **1a**-^{13}C and **1a**-^{15}N to 60 °C and monitored it by ^{1}H NMR spectroscopy (Scheme 1). During the reaction, no free azide was formed. After complete decomposition of the

Scheme 1

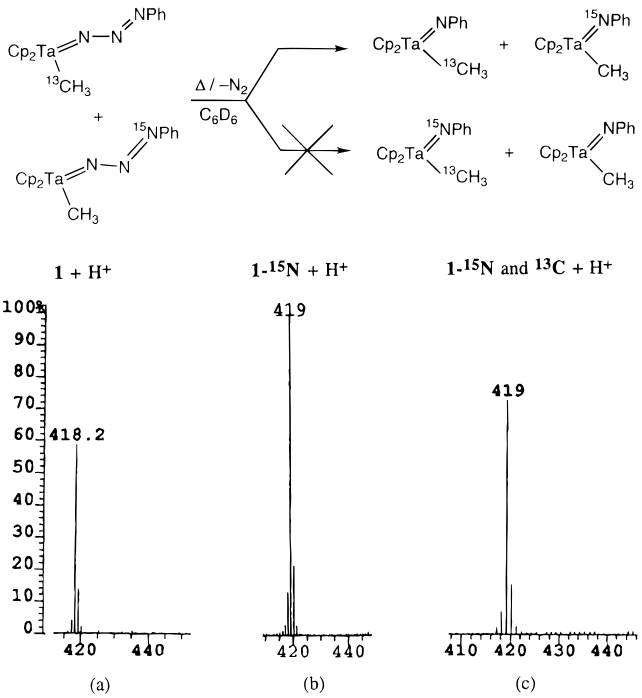

Figure 4. Mass spectral data for crossover experiment, including controls: (a) unlabeled **2a** made from thermally decomposed **1a**; (b) labeled **2a-^{15}N** prepared from independently made, thermally decomposed **1a-^{15}N**; (c) double-labeling crossover experiment showing only **2a-^{15}N** and **2a-^{13}C** made from a thermally decomposed 1:1 solution of **1a-^{15}N** and **1a-^{13}C**.

starting material, the only products detected were the singly labeled imido species, $Cp_2Ta(CH_3)(^{15}NPh)$ and $Cp_2Ta(^{13}CH_3)(NPh)$, in >97% yields determined by NMR and MS (FAB) analysis (the mass spectra are illustrated in Figure 4). No evidence for either the unlabeled ($Cp_2Ta(CH_3)(NPh)$) or doubly labeled ($Cp_2Ta(^{13}CH_3)(^{15}NPh)$) species in significant amounts was found.

We also attempted detailed kinetic studies on the rate of nitrogen loss in the conversion of **1a** to **2a**. Our initial attempts to measure the rate of the **1a** to **2a** reaction gave perplexing results. Although the reactions appeared to be approximately first order, erratic and irreproducible concentration vs time plots were obtained. Significantly, we found that exceedingly brief exposure of reaction solutions to the atmosphere caused significant accelerations in the rate, suggesting that the conversion was catalyzed by very small traces of air or water.

To deal with this problem, we added varying amounts of Cp_2ZrMe_2 to the solutions used for kinetic runs.[22] This material reacts rapidly with O_2 and H_2O to give soluble and NMR-observable $Cp_2(CH_3)ZrOZr(CH_3)Cp_2$, and so the presence of unreacted Cp_2ZrMe_2 remaining in solution provides strong assurance that the concentrations of air and water are extremely low.[12,14] Under these conditions, no reaction of the scavenger Cp_2ZrMe_2 with either **1a** or **2a** was observed, and the rates for the **1a** to **2a** conversion became slower and very well behaved.[15]

Using Cp_2ZrMe_2 as a water and/or O_2 scavenger, we investigated the rate of dinitrogen loss over a 40 °C temperature range. An example of the raw data is given in Figure 5 which shows the disappearance of $Cp_2Ta(CH_3)(N_3Ph)$ and the growth of $Cp_2Ta(CH_3)(NPh)$ at 69.2 °C. Also shown in Figure 6 are the raw data obtained at 69.2 °C plotted on a logarithmic scale showing clear first-order kinetics (k_{obs} at 69.2 °C was found to be (3.0 ± 0.1) × 10^{-4} s^{-1}). Rigorous first-order behavior (independent of the concentration of Cp_2ZrMe_2) was observed over a 40 °C temperature range, and an Eyring plot (shown in Figure 7) gave $\Delta H^{\ddagger} = 25.4 \pm 0.4$ kcal/mol and $\Delta S^{\ddagger} = -0.7 \pm 1.3$ eu.[23]

We have carried out a Hammett σ/ρ study using azidoaryl complexes having H (**1a**), NMe_2 (**1b**), and CF_3 (**1c**) substituents in the para positions of the aromatic ring (Figure 8). We were somewhat limited in the types of para substituents we could use because the tantalum starting material reacts rapidly with a wide range of substituents such as nitro, nitroso, hydroxy, cyano, and primary and secondary amines in an undesirable fashion. Despite this limitation on substituents, we still spanned a large electronic range, and an excellent linear log k vs σ plot was obtained. The ρ_{para} obtained for the reaction was +0.66, indicating that the reaction was accelerated by electron-withdrawing substituents.

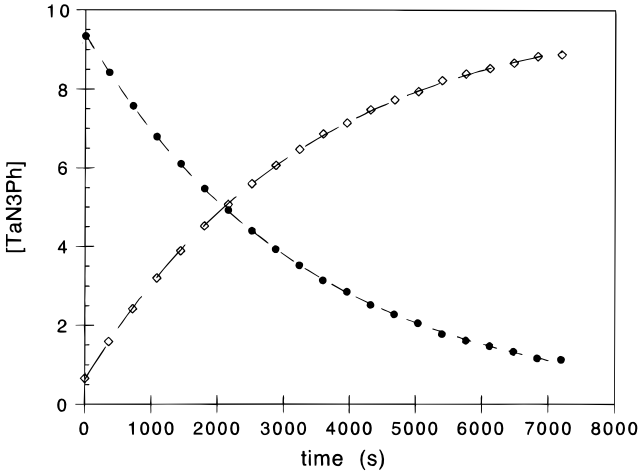

Figure 5. Kinetic data for the conversion of **1a** to **2a** at 69.2 °C in C_6D_6: ◇, [TaNPh]; ●, [TaN_3Ph].

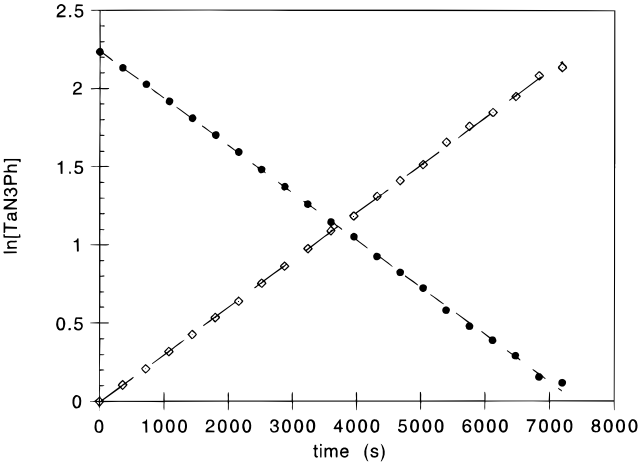

Figure 6. Kinetic data for the conversion of **1a** to **2a** at 69.2 °C in C_6D_6: ◇, ln[TaNPh]; ●, ln[TaN_3Ph].

(22) The crossover experiments described above were also carried out in the presence of Cp_2ZrMe_2 and the results shown to be independent of the additive.

(23) It is interesting that the analogous (arylazido)vanadium complex discovered by Cummins[15] is also converted to the corresponding arylimido complex, but the kinetics are second rather than first order. It is possible that this is due to the different electronic character of the vanadium species.

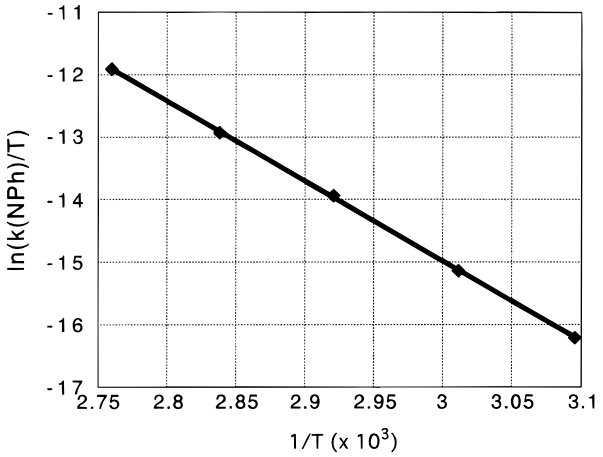

Figure 7. Eyring lot for the conversion of **1a** to **2a**. Activation parameters calculated from the plot: $\Delta H^{\ddagger} = 25.4$ kcal/mol; $\Delta S^{\ddagger} = -0.7$ cal/mol K.

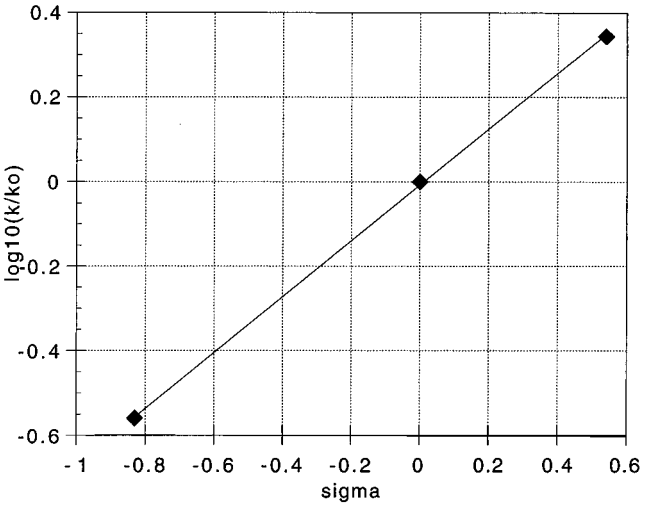

Figure 8. Hammett plot for the conversion of **1** to **2**. Rate constants were determined for X = CF_3, H, and NMe_2 at T = 79.2 °C in C_6D_6.

Discussion

Outlined in Scheme 2 are four possible nitrogen extrusion pathways for the conversion of **1** to **2**. The first possibility is similar to one proposed for the decomposition of organic azides in the presence of tertiary phosphines. These reactions are proposed to proceed through a reactive intermediate, R′NNNPR_3, that decomposes to dinitrogen and the corresponding phosphoranimine (eq 3). Earlier literature suggests that

$$PR_3 + N_3R' \longrightarrow R_3P{=}N{-}N{=}NR' \longrightarrow R_3P{=}NR' + N_2 \qquad (3)$$

these complexes, known as Staudinger phosphazides, decompose in a bimolecular fashion; however, the more recent literature points toward a unimolecular pathway.[24-26] Thus, the first possibility (pathway a in Scheme 2) is analogous to the bimolecular pathway first proposed for the Staudinger phosphazide decomposition where two molecules of **1a** dimerize and formally "trade" nitrene groups during the elimination of N_2.

The second possibility (pathway b in Scheme 2) is a unimolecular reaction that proceeds through a four-centered transition state. In this mechanism, the loss of dinitrogen involves cleaving the $N_\alpha-N_\beta$ bond and the Ph−N bond while a third $N_\beta-N_\gamma$ bond and a TaN−Ph

Scheme 2

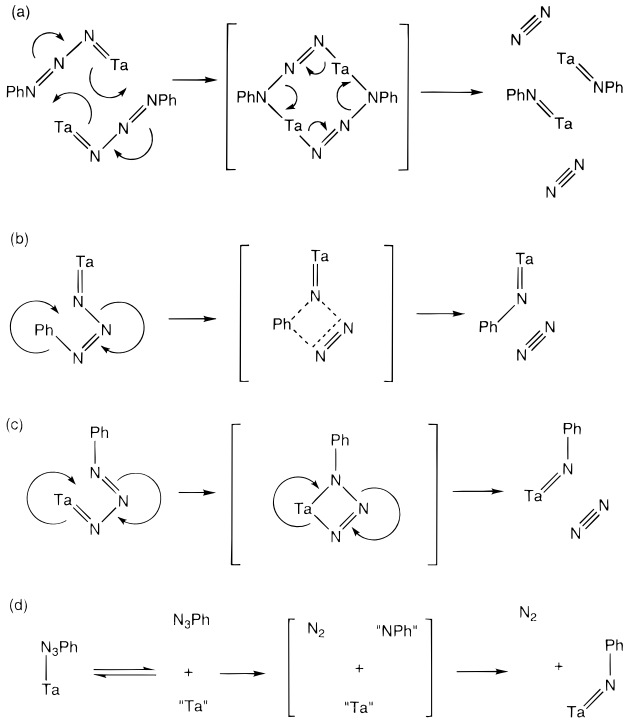

bond are formed. Essentially this involves metathesis of Ph−N bonds while the Ta=N bond is kept intact. Pathway c in Scheme 2 is also a unimolecular reaction with a four-centered transition state. However, this mechanism involves cleavage of the original Ta=N bond. Likewise, the Ph−N bond remains intact while the nitrogen atom bound to tantalum is extruded as N_2.

A fourth possibility (pathway d in Scheme 2) involves dissociation of the azide while free "Cp_2TaCH_3" is formed, and then the free azide decomposes to N_2 and a free nitrene ":NR". Following N_2 loss, the "naked" $Cp_2Ta(CH_3)$ recombines with the free nitrene to form the imido complex $Cp_2Ta(CH_3)(=NR)$.

Pathway a can be ruled out as a major mechanistic route because it does not appear to be consistent with the observed first-order kinetics or the lack of crossover in the double-labeling experiment (Scheme 1). We do not believe pathway b is the main decomposition route either since it is not supported by the single-labeling experiment (**1a**-^{15}N → **2a**-^{15}N), which conclusively shows that the Ph−N bond is not cleaved. Pathway d is inconsistent with the observed lack of crossover in the double-labeling experiment and the lack of scrambling of free azide to bound azide. However, it is difficult to rigorously rule out an extremely fast cage mechanism in which the recombination of Cp_2TaCH_3 with free nitrene occurs more rapidly than escape from the solvent sphere, though our kinetics do not point to this type of transition state.

The pathway that is most consistent with all of our observations is (c). This pathway allows for the formation of **2a**-^{15}N from **1a**-^{15}N by keeping the Ph−N bond intact while cleaving the Ta−N double bond. It is also consistent with the observed first-order kinetics and the lack of scrambling with respect to free and bound azide, and it explains the lack of observed crossover in the

(24) Gololobov, Y. G.; Kasukhin, L. F. *Tetrahedron* **1992**, *48*, 1353, and references therein.
(25) Mosby, W. L.; Silva, M. L. *J. Chem. Soc.* **1965**, 1003.
(26) Horner, L.; Gross, A. *Justus Liebigs Ann. Chem.* **1995**, *591*, 117.

Scheme 3

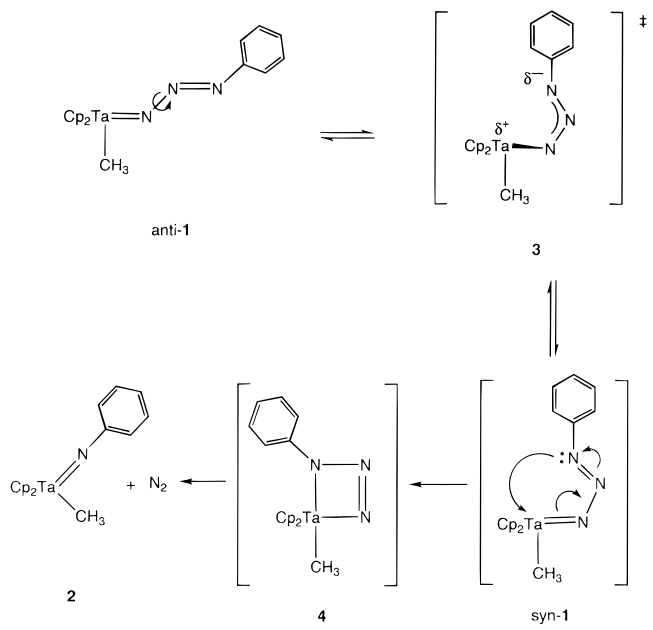

double-labeling experiment. The significant thermal barrier (25.4 ± 0.4 kcal/mol) and near-zero activation entropy ($\Delta S^{\ddagger} = -0.7 \pm 1.3$ eu) are consistent with a unimolecular reaction in which little free rotation is frozen out in proceeding from **1a** to the rate-determining transition state.

In the Hammett σ/ρ study designed to investigate the distribution of charge in the rate-determining transition state for the **1** → **2** conversion, we obtained a ρ_{para} value of +0.66. This number represents roughly a 1 order of magnitude change in the rate of N_2 elimination over the range from *p*-NMe_2 to *p*-CF_3. This was a surprising result, because we had assumed that the most likely mechanism for nitrogen loss would be rapid, reversible conformational isomerization of **1** (labeled anti-**1** in Scheme 3) to a syn isomer (syn-**1**) in which the terminal nitrogen of the azide ligand is located in closer proximity to the tantalum center. In a second (presumably rate-determining) step, the terminal nitrogen would attack at Ta, leading to a four-membered ring intermediate (**4**) that could rapidly lose N_2, leading to the imido complex **2**. However, if this mechanism were operating, the reaction rate should be slowed by electron-withdrawing substituents and accelerated by electron-donating substituents at nitrogen. Instead, we find the opposite trend. Therefore, we believe the Hammett study rules out a rate-determining step in which the lone pair electrons located at the terminal nitrogen atom attack the tantalum center.

As an alternative, we propose that the syn/anti isomerization is rate determining—i.e., that conversion of the stable anti conformation of **1** to its syn isomer is the slow step of the reaction and that N_2 loss is faster than reconversion of syn-**1** to anti-**1**. We then must deal with the question of why the syn/anti isomerization is accelerated by electron-withdrawing substituents on the azide ligand. To answer this question, we propose that the transition state for syn/anti isomerization has a structure like **3**, illustrated in Scheme 3. In this structure, the delocalized, diene-like Ta=N-N=NAr fragment is half-rotated, leading to a structure in which the Ta atom lies out of the plane of the three nitrogen atoms. This leads to a decrease in Ta−N d−π overlap and a substantial weakening of the Ta−N π-bond. We believe this loss of π-character is responsible for the main thermal barrier to N_2 loss. This transition state should be stabilized by charge separation in which negative charge builds up on the relatively electronegative "allyl-like" N_3 moiety, and positive charge is localized at the relatively electropositive Ta center.

This mechanism has precedent in the thermal decomposition of organic azo compounds. Substantial evidence exists that trans-azo compounds (which are analogous to anti-**1**) undergo N_2 loss substantially more slowly than cis azo compounds (analogous to syn-**1**). In small- and medium-sized cyclic azo compounds, in which cis stereochemistry is enforced by the ring structure, loss of dinitrogen occurs 100 times faster than it does in the analogous acyclic trans species.[27] It therefore seems reasonable that N_2 loss from anti- and syn-**1** might be characterized by a similar difference in rate.

Conclusions

As shown in Figures 2 and 3, we have synthesized and fully characterized several terminal (organoazido)-metal complexes, **1a-c**, from a tantalum−phosphine complex and organic azides. We have shown that these complexes in the solid state have slightly bent η^1-bound N_3R groups. Through a series of kinetic and labeling studies, we have been able to rule out bimolecular or dissociative mechanisms as well as phenyl group migration for the conversion of azido complex **1** to imido complex **2**. Our data support the hypothesis that dinitrogen loss occurs via a four-membered triazametallacyclobutene intermediate.

In probing the transition state for dinitrogen loss, the rate studies observed with para-substituted phenyl rings show that there is a significant accelerating effect caused by strongly electron-withdrawing groups. In order to account for this observation, we propose that the rate-determining transition state for the decomposition of **1** involves isomerization of the anti conformation of **1** to its syn isomer. This is then followed by attack of the terminal azide ligand nitrogen at Ta, followed by loss of dinitrogen, both of which are faster than return of syn-**1** to anti-**1**. We believe that the transition state for the rate-determining syn/anti isomerization is a "bent" or half-rotated isomer of the ground state which has the tantalum sitting out of the N_3Ar plane and negative charge buildup on the N_3 fragment in this species. This negative charge is most readily delocalized by electron-withdrawing groups, resulting in stabilization of the transition state and an acceleration of the overall decomposition rate.

Experimental Section

General Procedures. Unless otherwise noted, all reactions and manipulations were performed in dry glassware under a nitrogen atmosphere in a Vacuum Atmospheres HE-553-2 drybox equipped with a MO-40-2 Dri-train or using standard Schlenk techniques. Instrumentation at the University of California, Berkeley College of Chemistry X-Ray Crystallographic Facility (CHEXRAY) consists of two Enraf-Nonius CAD-4 diffractometers, each equipped with a nitrogen-flow low-temperature apparatus and controlled by a VAX II microcomputer. Both use Enraf-Nonius software are described in the CAD4 Operation Manual, Enraf-Nonius, Delft, Novem-

(27) Engel, P. S.; Bishop, D. J. *J. Am. Chem. Soc.* **1975**, *97*, 6754.

ber 1977, and updated thereafter. For descriptions of the NMR, IR, UV/visible, and mass spectral instruments as well as solvents and experimental techniques used, see an earlier paper from this group.[28] $Cp_2Ta(PMe_3)(CH_3)$,[16] C_6H_5-N_3,[10] *p*-CF_3-C_6H_4-N_3,[10] and *p*-$N(CH_3)_2$-C_6H_4-N_3[10] were prepared by literature methods.

$Cp_2Ta(CH_3)(N_3$-$C_6H_5)$ (1a). In the drybox, $Cp_2Ta(PMe_3)(CH_3)$ (127 mg, 0.316 mmol) was dissolved in freshly distilled, dry benzene (10 mL) and the resultant mixture was added to a large (20 mL) vial equipped with a stir bar. Next, a solution of PhN_3 (45.1 mg, 0.379 mmol) in benzene (5 mL) was added dropwise to the stirred solution, which immediately turned from deep red to orange. After the solution was stirred for 10 min, it was concentrated *in vacuo* to a slightly oily solid in order to remove PMe_3. At this point, the residue was redissolved in benzene (10 mL) and the solution was filtered through a 1-cm plug of freshly dried silylated silica gel (Keiselgel 60). The filtrate was then concentrated *in vacuo* to the point where solid began crystallizing out (~4 mL). Crystallization was completed by allowing slow vapor diffusion of pentane into the remaining benzene solution. The orange needlelike and platelike crystals of **1a** (124 mg, 88% yield) obtained by decanting the mother liquor were rinsed with pentane (2 × 3 mL). The crystals are stable indefinitely when stored in the dark at −35 °C. The presence of 0.5 equiv of benzene in the unit cell were confirmed by ^{1}H NMR spectroscopy and single-crystal X-ray diffraction analysis. Data for $Cp_2Ta(N_3Ph)(CH_3)$ (**1a**). Anal. Calcd for $C_{17}H_{18}N_3Ta(0.5\ C_6H_6)$: C, 49.60; H, 4.37; N, 8.68. Found: C, 49.37; H, 4.22; N, 8.31. mp = 105−8 °C dec; ^{1}H NMR (400 MHz, C_6D_6, 25 °C) δ 8.03 (dd, 2H, $^4J_{HH}$ = 1.2 Hz, $^3J_{HH}$ = 8.5 Hz, *o*-C_6H_5), 7.30 (t, 2H, $^3J_{HH}$ = 7.9 Hz, *m*-C_6H_5), 6.98 (t, 1H, $^3J_{HH}$ = 7.3 Hz, *p*-C_6H_5), 5.21 (s, 10H, C_5H_5), 0.54 (s, 3H, TaCH_3); ^{13}C{^{1}H} NMR (101 MHz, C_6D_6) δ 153.8 (s, *i*-C_6H_5), 129.2 (s, *o*-C_6H_5), 124.2 (s, *p*-C_6H_5), 121.0 (s, *m*-C_6H_5), 104.7 (s, C_5H_5), 4.1 (s, Ta-CH_3); ^{13}C NMR (101 MHz, C_6D_6) Ta-$^{13}CH_3$ δ 4.1 (q, $^1J_{CH}$ = 124.3 Hz); IR (KBr) 1730 ($\nu_{N=N}$) cm^{-1}; MS (FAB) *m*/*z* 418 ($M^+ + H - N_2$), 402 ($M^+ - N_2 - CH_3$).

$Cp_2Ta(CH_3)(N_3$-C_6H_4-*p*-$NMe_2)$ (1b). In the drybox, $Cp_2Ta(PMe_3)(CH_3)$ (60.0 mg, 0.149 mmol) was dissolved in freshly distilled, dry benzene (3 mL) and the resultant mixture was added to a large (20 mL) vial equipped with a stir bar. Next, a solution of *p*-$NMe_2C_6H_4N_3$ (30.7 mg, 0.189 mmol) in benzene (2 mL) was added dropwise to the stirred tantalum complex solution, which turned red-brown upon addition of the azide. The resulting mixture was immediately concentrated to ~1.5 mL *in vacuo*. The product was then crystallized by allowing slow vapor diffusion of pentane into the remaining benzene solution. The dark red needlelike crystals (64.7 mg, 89%) of **1b** obtained by decanting the mother liquor were rinsed with pentane (2 × 3 mL). Anal. Calcd for $C_{19}H_{23}N_4Ta$: C, 46.73; H, 4.75; N, 11.47. Found: C, 46.88; H, 4.73; N, 11.14. ^{1}H NMR (400 MHz, C_6D_6, 25 °C) δ 8.04 (d, 2H, $_3J_{HH}$ = 9.0 Hz, C_6H_4), 6.69 (d, 2H, $^3J_{HH}$ = 9.0, C_6H_4), 5.30 (s, 10H, C_5H_5), 2.51 (s, 6H, NCH_3), 0.64 (s, 3H, TaCH_3); ^{13}C{^{1}H} NMR (101 MHz, C_6D_6) δ 148.6 (s, NC_6H_4), 144.6 (s, NC_6H_4), 122.0 (s, C_6H_4), 113.7 (s, C_6H_4), 105.0 (s, C_5H_5), 40.7 (s, NCH_3), 4.1 (s, TaCH_3); IR (KBr, cm^{-1}) 2951 (w), 2919 (w), 2850 (w), 1733 (s), 1639 (m), 1500 (m), 1439 (s), 1381 (s), 1149 (m), 1018 (m), 814 (m).

$Cp_2Ta(CH_3)(N_3C_6H_4$-*p*-$CF_3)$ (1c). In the drybox, $Cp_2Ta(PMe_3)(CH_3)$ (65.2 mg, 0.162 mmol) was dissolved in freshly distilled, dry benzene (4 mL) and the resultant mixture was added to a large (20 mL) vial equipped with a stir bar. Next, a solution of *p*-$CF_3C_6H_4N_3$ (39.2 mg, 0.209 mmol) in benzene (1 mL) was added dropwise to the stirred solution. The resulting yellow solution was concentrated *in vacuo* to ~1.5 mL. The product was then crystallized by allowing slow vapor diffusion of pentane into the remaining benzene solution. The long, thin yellow needlelike crystals of **1c** obtained by decanting the mother liquor were dried *in vacuo* and isolated in 71.3 mg (86%) yield. These crystals are slightly less stable thermally than their counterparts **1a** and **1b** and are stored below room temperature in the dark. Anal. Calcd for $C_{18}H_{17}F_3N_3Ta$: C, 42.12; H, 3.34; N, 11.10. Found: C, 41.95; H, 3.46; N, 10.87. ^{1}H NMR (400 MHz, C_6D_6, 25 °C) δ 7.83 (d, 2H, $^3J_{HH}$ = 8 Hz, C_6H_4), 7.47 (d, 2H, $^3J_{HH}$ = 8 Hz, C_6H_4), 5.14 (s, 10H, C_5H_5), 0.46 (s, 3H, TaCH_3); ^{13}C {^{1}H} NMR (101 MHz, C_6D_6, 25 °C) δ 156.73 (s, *i*-C_6H_4), 126.45 (q, $^3J_{CF}$ = 4 Hz, *m*-C_6H_4), 120.43 (s, *o*-C_6H_4), 104.54 (s, C_5H_5), 4.33 (s, TaCH_3); ^{19}F{^{1}H} NMR (C_6D_6) δ −61.3 (s, CF_3); IR (KBr, cm^{-1}) 2944 (w), 2919 (w), 1730 (m), 1631 (s), 1596 (s), 1506 (s), 1434 (m), 1379 (s), 1315 (s), 1171 (m), 1153 (m), 1097 (m), 1060 (m), 821 (s), 677 (w).

Generation of Imido Complexes 2 from the Azide Species 1. For brevity, only generation of the parent imine is given since generation of the other complexes is identical. In the drybox, a toluene solution (5 mL) of $Cp_2Ta(CH_3)(N_3C_6H_5)$ (**1a**) (74.0 mg, 0.166 mmol) was heated to 80 °C for 7 h. The solution was concentrated *in vacuo* to a yellow glassy oil, and the product was left under full vacuum for 0.5 h to remove the last traces of solvent. The resulting oil was pure (>95% by ^{1}H NMR vs $FeCp_2$ internal standard) and had MS and ^{1}H NMR spectral characteristics identical to those reported in the literature.[17]

Sample Kinetic Run To Monitor the Rate of Dinitrogen Loss from 1a. In the drybox, $Cp_2Zr(CH_3)_2$ (0.4 mg, 1.6 μmol) and Cp_2Fe (0.4 mg, 2 μmol) were dissolved in freshly distilled C_6D_6, and the resultant solution was added to a NMR tube. Crystals of $Cp_2Ta(CH_3)(N_3C_6H_5)$ (**1a**) (4.2 mg, 9.4 μmol) were then added to the tube, which was shaken until all the crystals had dissolved. The tube was then attached to a Cajon fitting and removed from the box. After degassing the tube by three freeze−pump−thaw cycles, it was sealed and wrapped in foil. The tube was inserted into a prewarmed NMR probe at 49.9 °C (temperature calibrated vs external ethylene glycol standard). After temperature equilibration, a single-pulse ^{1}H NMR spectrum was taken every 20 min. Over the course of the reaction, there was no significant change in the concentration of the zirconocene scavenger.

Decomposition of 1a−^{15}N in the Presence of 1a-^{13}C. In the drybox, $Cp_2Zr(CH_3)_2$ (0.6 mg, 2.4 μmol) and Cp_2Fe (0.3 mg, 1 μmol) were dissolved in freshly distilled C_6D_6, and the resultant solution was added to a NMR tube. Crystals of $Cp_2Ta(CH_3)(NN^{15}NC_6H_5)$ (**1a-^{15}N**) (12.2 mg, 27.3 μmol) and $Cp_2Ta(^{13}CH_3)(N_3C_6H_5)$ (**1a-^{13}C**) (12.0 mg, 26.9 μmol) were then added to the tube. After the crystals dissolved, the tube was attached to a Cajon fitting and removed from the box. After degassing the tube by three freeze−pump−thaw cycles, it was sealed and wrapped in aluminum foil until the following step. The tube was inserted into a prewarmed NMR probe at 69.8 °C (temperature calibrated vs external ethylene glycol standard). The reaction was monitored by ^{1}H NMR spectroscopy, and no free azide species or intermediates were observed. After the dinitrogen loss was complete, ^{1}H and ^{13}C NMR analysis showed only **2a-^{15}N** and **2a-^{13}C**.[14] The tube was then brought back into the drybox and cracked open, and the solution was concentrated *in vacuo* to an oily solid. Mass spectral analysis also showed a spectrum identical to that obtained for a singly labeled **2a-^{15}N** control (See Figure 4).

X-ray Crystallographic Analysis of $Cp_2(CH_3)Ta(N_3C_6H_5)$ (1a). Orange needlelike and platelike crystals of the compound were obtained from benzene/pentane vapor diffusion as described above. Fragments cleaved from some of these crystals were mounted on glass fibers using Paratone N hydrocarbon oil. The crystals immersed in Paratone began almost immediately to give off bubbles (presumably N_2). The crystals were then transferred to an Enraf-Nonius CAD-4 diffractometer[29] and centered in the beam. They were cooled to −115 °C by a nitrogen-flow low-temperature apparatus which had been previously calibrated by a thermocouple placed at the sample position. Crystal quality was evaluated via

(28) Hostetler, M. J.; Butts, M. D.; Bergman, R. G. *J. Am. Chem. Soc.* **1993**, *115*, 2743.

(29) Calculations were performed on DEC MicroVax computers using locally modified versions of the Enraf-Nonius Mo1EN structure solution and refinement package and other programs.

measurement of intensities and inspection of peak scans until a suitable sample was found. Automatic peak search and indexing procedures yielded a monoclinic reduced primitive cell. Inspection of the Niggli values[30] revealed no conventional cell of higher symmetry. The final cell parameters and specific data collection parameters for this data set are given in Table 1.

The 2486 raw intensity data were converted to structure factor amplitudes and their esd's by correction for scan speed, background, and Lorentz and polarization effects.[29] Inspection of the intensity standards revealed a reduction of 8% of the original intensity. The data were corrected for this decay. Inspection of the azimuthal scan data[29] showed a variation $I_{min}/I_{max} = 0.63$ for the average curve. An empirical correction based on the observed variation was initially applied to the data. However, following refinement, it appeared that this had overcorrected the data and an empirical correction was made to the data based on the combined differences of F_o and F_c following refinement of all atoms with isotropic thermal parameters ($T_{max} = 1.12$, $T_{min} = 0.86$, no θ dependence).[31] Inspection of the systematic absences indicated possible space groups $P2_1$ and $P2_1/m$. The choice of the acentric group $P2_1$ was confirmed by the successful solution and refinement of the structure. Removal of systematically absent data left 2462 unique data in the final data set.

The structure was solved by Patterson methods in space group $P2_1$ and refined via standard least-squares and Fourier techniques. In a difference Fourier map calculated following the refinement of all non-hydrogen atoms with anisotropic thermal parameters, peaks were found corresponding to the positions of some of the hydrogen atoms. Hydrogen atoms were assigned idealized locations and values of $B_{iso} \sim 1.3$ times the B_{eqv} of the atoms to which they were attached. They were included in structure factor calculations but not refined. In the final cycles of least-squares refinements, 18 data with abnormally large weighted difference values were given zero weight. The absolute configuration of the crystal was tested by refining both enantiomorphs with Ta anisotropic and all other atoms isotropic ($\Delta R = 0.13\%$). Refinement refused to converge for the thermal parameters on N_4 so it was finally refined with an isotropic thermal parameter.

The final residuals for 427 variables refined against the 2277 accepted data for which $F^2 > 3\sigma(F^2)$ were $R = 2.36\%$, $wR = 2.82\%$, and GOF = 1.297. The R value for all 2462 data was 2.75%.

The quantity minimized by the least-squares program was $\Sigma w(|F_o| - |F_c|)^2$, where w is the weighted of a given observation. The p-factor used to reduce the weight of intense reflections was set to 0.03 throughout the refinement. The analytical forms of the scattering factor tables for the neutral atoms were used and all scattering factors were corrected for both the real and imaginary components of anomalous dispersion.

Inspection of the residuals ordered in ranges of sin θ/λ, $|F_o|$, and parity value of the individual indexes showed no unusual features or trends. The largest peak in the final difference Fourier map had an electron density of 0.65 $e^-/Å^3$, and the lowest excursion was -0.19 $e^-/Å^3$. There was no indication of secondary extinction in the high-intensity, low-angle data.

The positional and thermal parameters of the non-hydrogen atoms are given in Table 2. Anisotropic thermal parameters and the positions and thermal parameters of the hydrogen atoms, as well as a listing of the values of F_o and F_c, are available as supplementary material.

X-ray Crystallographic Analysis of $Cp_2(CH_3)Ta(N_3C_6H_4$-*p*-$NMe_2)$ (1b). Red columnar crystals of the compound were obtained by slow crystallization from benzene/pentane vapor diffusion, mounted, and centered in the X-ray beam as described above for **1a**. They were cooled to -111 °C by a nitrogen-flow low-temperature apparatus, which had been previously calibrated by a thermocouple placed at the sample position. Preliminary analysis was also carried out as described for **1a**. The final cell parameters and specific data collection parameters for this data set are given in Table 1 for the conventional setting of the cell for space group $Pna2_1$.

The 2996 raw intensity data were converted to structure factor amplitudes and their esd's by correction for scan speed, background, and Lorentz and polarization effects.[29] No correction for crystal decomposition was necessary. Inspection of the azimuthal scan data showed a variation $I_{min}/I_{max} = 0.45$ for the average curve. An empirical correction based on the observed variation was applied to the data. Inspection of the systematic absences indicated possible space groups $Pna2_1$ and $Pnma$. The choice of the acentric group $Pna2_1$ was confirmed by the successful solution and refinement of the structure. Removal of systematically absent and averaging of redundant data ($R_I = 2.7\%$) left 1456 unique data in the final data set.

The structure was solved by Patterson methods and refined via standard least-squares and Fourier techniques. In a difference Fourier map calculated following the refinement of all non-hydrogen atoms with anisotropic thermal parameters, peaks were found corresponding to the positions of most of the hydrogen atoms. Hydrogen atoms were assigned idealized locations and values of $B_{iso} \sim 1.25$ times the B_{eqv} of the atoms to which they were attached. They were included in structure factor calculations but not refined. The enantiomorph was tested by refining both the obverse and inverse structures.

The final residuals for 216 variables refined against the 1143 data for which $F^2 > 3\sigma(F^2)$ were $R = 1.53\%$, $wR = 1.70\%$, and GOF = 0.69. The R value for all 1456 data was 2.71%. Data analysis was carried out as described for **1a**. The largest peak in the final difference Fourier map had an electron density of 0.39 $e^-/Å^3$, and the lowest excursion was -0.38 $e^-/Å^3$. There was no indication of secondary extinction in the high-intensity, low-angle data.

The positional and thermal parameters of the non-hydrogen atoms are given in Table 4. Anisotropic thermal parameters and the positions and thermal parameters of the hydrogen atoms, as well as a listing of the values of F_o and F_c, are available as supporting information.

Acknowledgment. We thank Prof. Christopher C. Cummins and his co-workers for helpful discussions and for their willingness to disclose results of their independent investigation prior to publication. We are also grateful to Prof. Paul S. Engel for helpful discussions on the mechanism of organic azo compound thermolysis, and to a reviewer for several mechanistic suggestions. We acknowledge the National Science Foundation (Grant CHE-9416833) for generous financial support of this work and Dr. F. J. Hollander, director of the U.C. Berkeley X-ray diffraction facility (CHEXRAY), for determination of the X-ray structure. G.P. thanks the Department of Education for a predoctoral fellowship.

Supporting Information Available: Tables containing anisotropic thermal parameters and the position and thermal parameters of the hydrogen atoms for **1a** and **1b** (14 pages). NMR spectra for **1** in the presence of $Cp_2Zr(CH_3)_2$ are already on file.[14] This material is contained in many libraries on microfiche, immediately follows this article in the microfilm version of the journal, and can be ordered from the ACS; see any current masthead page for ordering information.

OM950796O

(30) Roof, R. B. J. *A Theoretical Extension of the Reduced-Cell Concept in Crystallography*; Publication LA-4038; Los Alamos Scientific Laboratory: Los Alamos, NM, 1969.

(31) Walker, N.; Stuart, D. *Acta Crystallogr.* **1983**, *A39*, 159.